ACS APPLIED MATERIALS & INTERFACES

Research Article

www.acsami.org

Virus-Mimicking Optical Nanomaterials: Near Infrared Absorption and Fluorescence Characteristics and Physical Stability in Biological Environments

Bongsu Jung and Bahman Anvari*

Department of Bioengineering, University of California—Riverside, Riverside, California 92521, United States

ABSTRACT: The use of viruses as platforms for the development of optical imaging materials has received increasing attention in recent years. We have engineered a hybrid nanomaterial composed of the capsid proteins of genome-depleted plant-infecting Brome mosaic virus that encapsulates the near-infrared (NIR) dye indocyanine green. Herein, we investigate the NIR absorption and fluorescence characteristics of these nanomaterials in biological environments consisting of cell culture media with and without serum proteins. Our results demonstrate that the NIR absorption and fluorescence emission of the constructs are enhanced in the presence of serum proteins. The constructs remain physically stable and maintain their NIR absorption and fluorescence properties for at least 79 days. The presence of serum proteins also reduces the aggregation of the constructs. These findings have relevance for the further development of optical imaging and phototherapeutic methods on the basis of such virus-mimicking nanomaterials as well as the expected optical and physical characteristics of these nanomaterials in vivo.

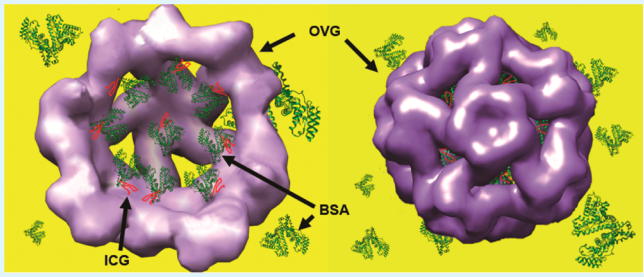

KEYWORDS: *albumin, indocyanine green, hybrid materials, imaging, nanoparticles, nanotechnology, serum*

INTRODUCTION

Optical nanosized materials present a promising technology for imaging a wide range of diseases at the cellular and molecular levels.[1−4] In particular, the use of such materials with capabilities for near-infrared (NIR) (≈700−1000 nm) fluorescence imaging offers some advantages: (1) due to the reduced absorption of photons by water and proteins as well as the diminished scattering within the NIR spectral band,[5] these wavelengths allow for relatively deep optical penetration (on the order of a cm) and (2) given that there is negligible tissue autofluorescence in the NIR spectral band, an exogenous NIR optical material as a contrast agent can enhance the signal-to-background ratio.

Quantum dots (QDs) are inorganic (semiconductor) materials with tunable NIR emission.[4,6−8] Although they have relatively high fluorescence quantum yields, strong resistance to photobleaching, and low chemical degradation compared with organic fluorophores,[9,10] their potential biomedical imaging applications remain limited because of cytotoxicity resulting from heavy-metal elements (Cd, Se).[9,11,12]

Nanoparticle (NP)-based imaging using organic NIR dyes presents an alternative approach. Various materials including liposomes,[13] low-density lipoprotein (LDL),[14] micelles,[15−17] and synthetic polymers[18−22] have been used to encapsulate organic dyes.

More recently, the use of biological materials, such as those derived from viruses as platforms to encapsulate imaging agents, has gained increased attention by many investigators. There are some advantages in using virus-mimicking particles (VMPs): (1) their fabrication can be achieved by self-assembly mechanisms,[23,24] (2) VMPs are highly monodispersed,[23,25] (3) VMPs derived from plant viruses may potentially be safe and biocompatible,[26,27] and (4) the presence of naturally available chemical functional groups on the viral capsid surface, such as amines, provides addressable sites for the functionalization of VMPs with targeting moieties.[28−32]

Various materials have been encapsulated into VMPs or conjugated onto their surfaces. Inorganic materials such as QDs,[33] negatively charged gold,[34,35] and magnetic[36] nanoparticles have been encapsulated by protein-based cages derived from Ross River virus (RRV) and Brome mosaic virus (BMV). Organic dyes have been conjugated onto the external surface of VMPs. For example, non-NIR fluorescent dyes such as Alexa Fluor 555, 488, and 647 were conjugated onto the surface of Cowpea mosaic virus (CPMV)[37] and Potato virus X (PVX)[38] and used for vascular and cellular imaging. The positively charged dye rhodamine and anticancer drug doxorubicin have been infused into Red clover necrotic mosaic virus (RCNMV) via opened pores within the capsid.[39] Recently, we provided the first report of utilizing the capsid protein (CP) subunits of plant-infecting BMV to encapsulate indocyanine green (ICG), which is the only FDA-approved NIR dye.[23] We refer to these hybrid nanostructures as optical viral ghosts (OVGs) because

Received: May 13, 2013
Accepted: July 22, 2013
Published: July 22, 2013

the genomic content of the wild-type BMV is removed and replaced by ICG.

As a first step toward understanding the optical characteristics of OVGs in biological environments, we report the effects of serum proteins on (1) the absorption and fluorescence characteristics of OVGs, (2) the stability of OVGs over a relatively long time period (79 days), and (3) the aggregation of OVGs. Serum proteins are particularly important biological molecules because they can be readily adsorbed on the surface of NPs within the vasculature and alter their physical and chemical properties.[40−46]

We incubated the OVGs in McCoy's 5a cell culture medium, a general purpose medium that supports the propagation of many types of primary cells and established cell lines,[47] with various levels of fetal bovine serum (FBS). We began by a series of spectroscopic studies to investigate the effects of FBS on nonencapsulated ICG as the control benchmark. We then performed similar studies using bovine serum albumin (BSA) and nonencapsulated ICG to test our hypothesis that albumin is one of the major serum proteins in FBS responsible for the observed effects. Once we determined the effects of FBS and BSA on nonencapsulated ICG as the control benchmark, the next step in our experimental strategy was to investigate the effects of FBS and BSA on OVGs, which is a key focus of this study.

We demonstrate that the presence of FBS increases the absorption and fluorescence of OVGs in specific NIR spectral bands. Additionally, the presence of FBS helps maintain the enhanced absorbance over an extended time interval (79 days) and reduces the aggregation of OVGs. To the best of our knowledge, these are the first results in relation to the optical and physical characteristics of OVGs in a biological environment. The significance of these findings is in relation to the development of future optical imaging and phototherapeutic methods on the basis of OVGs as well as the expected optical and physical characteristics of these nanomaterials in vivo.

RESULTS AND DISCUSSION

Effects of FBS and Bovine Serum Albumin (BSA) on the Absorbance and Fluorescence Emission Characteristics. We first investigated the effects of FBS on the absorption and fluorescence emission properties of nonencapsulated ICG as the control benchmark material in OVG suspension buffer (pH 4.3, ionic strength (I) = 0.074 mol/L). Without FBS, the absorption peak of ICG (13 μM) at 704 nm was dominant (Figure 1a). This peak is associated with the dimeric form of ICG (H-like aggregate).[48,49] The absorption peak of ICG at 780 nm is associated with the monomeric form of ICG,[48] with an absorbance (A) value of approximately 0.7 (Figure 1a).

In the absence of FBS, the wavelength (λ) dependent, effective molar extinction coefficient ($\varepsilon(\lambda)$) of ICG molecules, which is directly related to A, can be expressed as

$$\varepsilon(\lambda) = f_M \varepsilon_M(\lambda) + f_H \varepsilon_H(\lambda) \quad (1)$$

where f_M and f_H are the respective fractions of the monomeric and H-like aggregate forms of ICG in OVG buffer solution without FBS and $\varepsilon_M(\lambda)$ and $\varepsilon_H(\lambda)$ are the respective molar extinction coefficients of the monomeric and H-like aggregate forms of ICG in OVG buffer solution without FBS. For a fixed ICG concentration (13 μM), when FBS at 5 and 10% levels were added to the OVG suspension buffer, the monomeric A value increased to 1.5 and 1.66, respectively (Figure 1a).

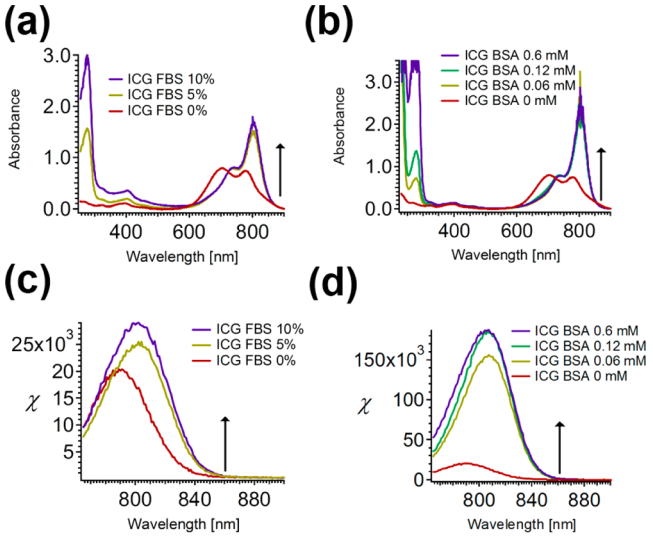

Figure 1. Effects of FBS and BSA on the absorption and normalized fluorescence emission (χ) spectra of ICG (13 μM) in OVG suspension buffer (pH 4.3, I = 0.074 mol/L). Panels a and b correspond to the absorption spectra in the presence of FBS and BSA at various levels, respectively. Panels c and d correspond to the normalized fluorescence emission spectra of ICG in response to 750 nm excitation with different levels of FBS and BSA, respectively. The arrows indicate the direction of the increasing levels of FBS or BSA.

However, the A value associated with H-like aggregates remained nearly constant (≈0.8) with and without supplemental FBS.

We attribute the FBS-induced enhancements in the monomeric A value to the presence of BSA in FBS. Because the molecular structure of BSA is similar to that of human serum albumin (HSA) (with the exception of BSA having two tryptophan residues whereas HSA has only one[50,51]), the interactions between ICG and BSA are expected to be similar to those between HSA and ICG. Other investigators have reported that 1 to 2 ICG molecules bind to the hydrophobic core of HSA.[52−55] Therefore, when ICG molecules were introduced into OVG suspension buffer containing FBS, they bound to BSA as monomers at their designated binding sites. The effective molar extinction coefficient of ICG molecules in presence of BSA, $\varepsilon^{BSA}(\lambda)$, can be expressed as

$$\varepsilon^{BSA}(\lambda) = f_M^{BSA} \varepsilon_M(\lambda) + f_H^{BSA} \varepsilon_H(\lambda) + \sum_{i=1}^{n} f_{M_i}^{*BSA} \varepsilon_{M_i}^{*BSA}(\lambda) \quad (2)$$

where f_M^{BSA} and f_H^{BSA} are the respective fractions of the unbound monomeric and H-like aggregate forms of ICG in OVG buffer solution containing BSA, $f_{M_i}^{*BSA}$ is the fraction of the ICG monomers bound to BSA with index i representing the number of monomers (i.e., 1, 2) binding to BSA, and $\varepsilon_{M_i}^{*BSA}(\lambda)$ is the molar extinction coefficient of the bound ICG monomers. Therefore, in the presence of BSA, the effective molar extinction of ICG includes the contributions from both the unbound and BSA-bound forms of the ICG monomers, with each having its own respective molar extinction coefficient and relative fraction, which collectively give rise to the enhanced A value of the monomeric form. The increase in fluorescence emission intensity of the monomeric form can subsequently be explained on the basis of the corresponding increase in absorbance. The observation that the A value associated with

H-like aggregates remained almost unaltered suggests that the product of the molar extinction coefficient associated with H-like aggregates, $\varepsilon_H(\lambda)$, and the fraction of aggregates, f_H^{BSA}, was not affected in the presence of BSA.

In the presence of 5 and 10% FBS, the absorption spectra in the range of ≈630−850 nm were bathochromically (red) shifted. In particular, there was a bathochromic shift in the monomeric absorption peak from 780 to 804 nm (Figure 1a). Our observed bathochromical shifts in the ICG absorption spectra in the presence of FBS are consistent with those reports by other investigators.[48,56,57]

We use the exciton theory for molecular assemblies to explain the origin of the spectral peak shifts associated with absorption by the ICG monomeric form.[58,59] In accordance with this theory, the excitonic state of the bound monomer form of ICG can split into two levels (E' and E''), with the exciton-splitting energy defined as $\Delta E = E'' - E'$. The lower excited state, E', is produced by the in-phase arrangement of the transition dipoles in the bound forms of ICG. Photoexcitation of the bound ICG monomer will produce a transition from the ground state to E' and therefore a bathochromic shift.

To test our hypothesis that the enhanced and bathochromically shifted monomeric absorbance of ICG in the presence of FBS can be attributed to ICG binding to BSA, we present the absorption spectra of ICG in OVG suspension buffer at various BSA levels (Figure 1b). In the presence of BSA and even at its lowest applied concentration (0.06 mM), the monomeric A value reached the saturation level of 2.1. This result is consistent with our hypothesis that albumin is the major contributor in FBS to amplifying the monomeric absorption of ICG, which we explain on the basis of ICG binding to specific sites on albumin. Because 0.06 mM BSA was sufficient to induce a saturation effect, we learn from the overlapping NIR spectra associated with various BSA levels that ICG at the applied concentration of 13 μM already occupied the available BSA binding sites, and additional increases in BSA concentration did not result in further interactions with ICG. Similar to the ICG absorption spectra in the presence of FBS, a bathochromic shift in the monomer absorption was induced by BSA. Higher concentrations of BSA resulted in corresponding increased absorbance levels at 279 nm, which is the signature absorption peak of BSA (Figure 1b).

We present the influence of FBS on the fluorescence emission of ICG in OVG suspension buffer (Figure 1c). In response to 750 nm excitation, the fluorescence spectra of ICG in OVG suspension buffer without supplemental FBS showed emission from the monomer form of ICG with peak intensity at 790 nm. The presence of FBS leads to the binding of ICG monomers to BSA, resulting in bathochromic shifts and an enhanced fluorescence emission intensity (Figure 1c). We observed similar bathochromic shifts and enhanced fluorescence emission intensities of ICG when BSA was added to the OVG suspension buffer (Figure 1d). These results confirmed that the observed bathochromic shifts and enhancements in both monomer absorption and fluorescence emission intensity in the presence of FBS were due to BSA binding to ICG.

Philip et al. have reported similar enhancements of the monomeric fluorescence emission of ICG in the presence of HSA.[48] In another study, the fluorescence emission of cypate was reported to increase in the presence of BSA.[60] When OrgG, Alexa488, RhodG, and TexRed dyes were dissociated by sodium dodecyl sulfate treatment, the monomeric absorbance and fluorescence were enhanced, suggesting that the disruption of the aggregate forms of the dyes is a major mechanism to the observed enhancements.[61]

Upon encapsulation into the viral capsid-based constructs, the spectral peak associated with ICG monomer absorption was bathochromically shifted by approximately 20 nm (compare the absorption spectrum associated with FBS 0% in Figure 1a with the spectra in Figure 2a). The presence of a sulfonate group

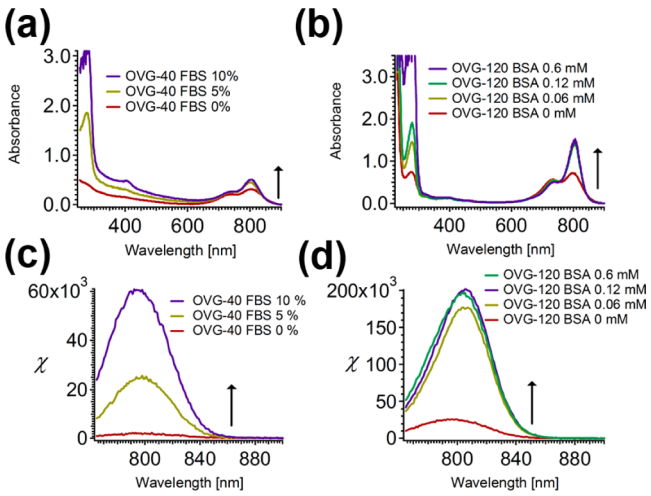

Figure 2. Effects of FBS and BSA on the absorption and normalized fluorescence emission spectra of OVGs suspended in OVG buffer (pH 4.3, I = 0.074 mol/L). Panels a and c correspond to the absorption and normalized fluorescence emission spectra, respectively, of OVG-40 constructs in the presence of FBS at various levels. Panels b and d correspond to the absorption and normalized fluorescence emission spectra, respectively, of OVG-120 constructs in the presence of BSA at various levels. Fluorescence spectra were obtained in response to a 750 nm excitation wavelength. The arrows indicate the direction of the increasing levels of FBS or BSA.

bound to the nitrogens of each polycyclic part results in a net negative charge and the water solubility of ICG. This negatively charged and hydrophilic part of ICG can electrostatically bind to positively charged amino acids such as arginine and lysine in the N-terminal arm of the BMV CP subunits.[23,62]

When ICG is incorporated into the OVG constructs, an ensemble of ICG conformational states composed of unbound ICG monomers, H-like aggregates, and monomers bound to CP subunits can form. We express the effective molar extinction coefficient of ICG molecules within the OVG constructs, $\varepsilon_{OVG}(\lambda)$, as

$$\varepsilon_{OVG}(\lambda) = f_{M_{OVG}}\varepsilon_{M_{OVG}}(\lambda) + f_{H_{OVG}}\varepsilon_{H_{OVG}}(\lambda) + \sum_{i=1}^{n} f^{*CP}_{M_{OVG_i}}\varepsilon^{*CP}_{M_{OVG_i}}(\lambda) \quad (3)$$

where $f_{M_{OVG}}$ and $f_{H_{OVG}}$ are the respective fractions of the unbound monomeric and H-like aggregate forms of ICG within the OVG constructs, $\varepsilon_{M_{OVG}}(\lambda)$ and $\varepsilon_{H_{OVG}}(\lambda)$ are the respective molar extinction coefficients of the unbound monomeric and H-like aggregate forms of ICG within the OVB constructs, $f^{*CP}_{M_{OVG_i}}$ is the fraction of ICG monomers bound to the CP subunits of the OVGs with index i representing the number of monomers, and $\varepsilon^{*CP}_{M_{OVG_i}}(\lambda)$ is the molar extinction coefficient of ICG monomers bound to CP subunits. The excitonic state of

the bound ICG monomer in the OVG constructs can split into two levels. Subsequent photoexcitation leads to a transition from the ground state to the lower energy state, E', inducing a bathochromic shift.

In the absence of FBS, the monomeric A value of the OVG-40 construct was approximately 0.3 (Figure 2a). When FBS at 5 and 10% levels were added to the OVG suspension buffer, the monomeric A value increased to 0.4 and 0.5, respectively (Figure 2a). However, the A value associated with H-like aggregates remained in the range of 0.20−0.26 with and without supplemental FBS. Similarly, the monomeric A value of OVG-120 increased from 0.7 (without BSA) to 1.4 (BSA in the range of 0.06−0.6 mM) (Figure 2b). There were no further FBS- or BSA-induced bathochromic shifts in the absorbance of the OVG-40 and OVG-120 constructs beyond what was already induced by the encapsulation of ICG into the constructs. Consistent with the enhanced fluorescence emission intensity of free ICG in the presence of BSA or FBS, we observed a similar enhancement with OVGs when FBS or BSA were added to the OVG suspension buffer (Figure 2c,d).

To confirm that these absorbance and fluorescence enhancements were not due to the interaction between BSA and the ICG molecules leaked from OVGs, we obtained the spectra immediately after suspending the OVGs in the BMV suspension buffer (pH 4.3, I = 0.074 mol/L). At pH 6−8 and I > 1.0 mol/L, the CP subunits of the BMVs become disassembled, and their RNA contents are released.[63] However, BMVs remain physically stable at lower pH and I values.[63−67] Therefore, OVGs are stable in the suspension buffer. In our previous study, we demonstrated that there was no ICG leakage for at least 5 h when OVGs were in the OVG suspension buffer.[23]

The absorbance and fluorescence enhancement of OVGs can result from the presence of FBS, which is mostly composed of BSA (66 kDa, 2.5 nm),[68−70] within the OVG constructs. Virus structures are known to be porous and have a cavity. Previous studies based on neutron small-angle scattering and electron microscopy indicate that there is a central hole (cavity) ranging between 4 and 10 nm for wild-type BMV[71−74] with a T = 3 icosahedral structure.[75,76] It is known that BMV T = 1 (and possibly T = 3) structures have large pores (2 to 3 nm) connected to the cavity at the threefold axes.[77,78] Analogous to BMV, the Cowpea chlorotic mottle virus (CCMV), which is a member of Bromoviridae family that includes the BMV and Bean mottle virus[79,80] has 60 pores of approximately 2 nm in diameter at the quasi-threefold axes.[81,82] These surface pores allow ions and molecules to gain access to the interior cavity of the virus.[30,83] Similarly, the MS2 bacteriophage contains 32 pores of 1.8 nm in diameter at the fivefold and threefold axes.[84,85] Red clover necrotic mosaic virus (RCNMV) also has pores at the quasi-threefold axes.[39,86] Loo et al. demonstrated that rhodamine and doxorubicin could be infused into the interior cavity of RCNMV via the surface pores.[39]

We present a transmission electron microscope image of OVG-4 constructs prepared by negative staining with 2% uranyl acetate (Figure 3). The presence of the negative stain indicates that the uranyl acetate infiltrated into the OVG construct. This observation suggests that the structure of OVGs is similar to the T = 1 BMV structure containing surface pores,[77,87] through which uranyl acetate can infiltrate and gain access into the cavity of the OVGs. In a similar manner, BSA can access the interior cavity of OVG via the surface pores and interact with ICG. In particular, the interaction can be between the two

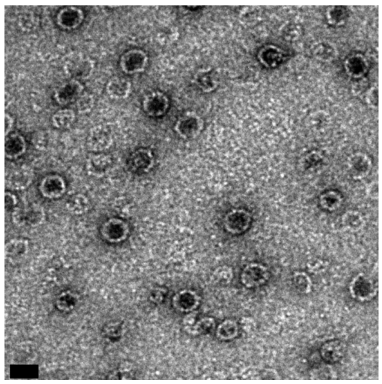

Figure 3. Transmission electron microscope image of OVG-4 constructs. OVGs were negatively stained with 2% uranyl acetate. Scale bar = 25 nm.

polycyclic (benzoindotricarbocyanine) lipophilic moieties of ICG and the hydrophobic components of BSA.

In the presence of BSA, the effective molar extinction of ICG molecules within the OVG constructs, $\varepsilon_{OVG}^{BSA}(\lambda)$, can be expressed as

$$\varepsilon_{OVG}^{BSA}(\lambda) = f_{M_{OVG}}^{BSA}\varepsilon_{M_{OVG}}(\lambda) + f_{H_{OVG}}^{BSA}\varepsilon_{H_{OVG}}(\lambda) + \sum_{i=1}^{n} f_{M_{OVG_i}}^{*CP}\varepsilon_{M_{OVG_i}}^{*CP}(\lambda) + \sum_{i=1}^{n} f_{M_{OVG_i}}^{*BSA}\varepsilon_{M_{OVG_i}}^{*BSA}(\lambda) + \sum_{i=1}^{n} f_{M_{OVG_i}}^{*CP*BSA}\varepsilon_{M_{OVG_i}}^{*CP*BSA}(\lambda) \quad (4)$$

where $f_{M_{OVG}}^{BSA}$ and $f_{H_{OVG}}^{BSA}$ are the respective fractions of the unbound monomeric and H-like aggregate forms of ICG in the presence of BSA within the OVG constructs, $f_{M_{OVG_i}}^{*BSA}$ is the fraction ICG monomers bound to BSA within the OVGs, $\varepsilon_{M_{OVG_i}}^{*BSA}(\lambda)$ is the molar extinction coefficient of the ICG monomers bound to BSA within the OVG constructs, $f_{M_{OVG_i}}^{*CP*BSA}$ is the fraction of the monomeric forms of ICG bound to both the CP subunits and BSA simultaneously (e.g., the hydrophilic part of ICG binding to the CP subunits and the lipophilic part of ICG binding to BSA), and $\varepsilon_{M_{OVG_i}}^{*CP*BSA}(\lambda)$ is the molar extinction coefficient of the monomeric forms of ICG that simultaneously may bind to CP subunits and BSA.

On the basis of eq 4, the relative fractions of the unbound and bound forms of the ICG monomers within the OVG constructs as well as their corresponding molar extinction coefficients can change in such a manner as to cause an increase in the absorbance value at the spectral peak associated with the monomer form in the presence of FBS or BSA (Figure 2a,b). Subsequently, the enhancement in the fluorescence emission intensity of the monomer form in the presence of FBS or BSA can be attributed to the corresponding increase in the monomeric absorbance. Given that the presence of BSA enhanced the absorbance of the ICG monomers (Figure 2b), without inducing further spectral shifts beyond those already brought about by the interaction between the ICG monomers and CP subunits, we suggest that the molecular dipoles and polarizability of ICG within the OVG constructs were not further altered in the presence of BSA to induce additional changes in the excitonic state of the ICG monomers.

Physical and Optical Stability of OVGs. Without any centrifugation, OVGs in an Eppendorf tube precipitated after 24 h of incubation in cell culture medium supplemented with FBS 5% at 4 °C in the dark (Figure 4a). The precipitation of

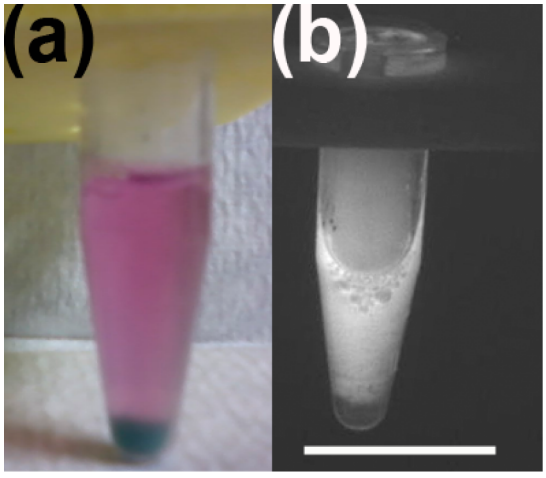

Figure 4. Brightfield (a) and NIR fluorescence (b) images of OVG-10 constructs after 24 h of incubation in McCoy's 5A cell culture medium with 5% supplemental FBS at 4 °C in the dark. Scale bar = 20 mm.

OVGs into a pellet suggests that the constructs remained intact and did not dissociate after incubation in cell culture medium. As indicated earlier, the CP subunits of BMV become dissociated at pH > 6 and I > 1 mol/L.[63] Although the pH of the cell culture medium is 7.4, its ionic strength (I) of 0.13 mol/L is substantially lower than the threshold value above which the CP subunits become dissociated.[63] In addition to the observed precipitation of OVGs, the fluorescence of this set of OVGs, which were intentionally fabricated to be minimal, was not detectable by the CCD camera and is shown as the dark image of the pellet (Figure 4b). This persistent dark image presents another evidence that the OVGs remained intact and were not fragmented in the cell culture medium after 24 h of incubation (although there was some ICG leakage into the cell culture medium). Therefore, the cell culture medium's relatively low value of I was effective in keeping the OVGs intact. OVGs remained precipitated at the bottom of the Eppendorf tube after 79 days of incubation in the cell culture medium without and with 5 and 10% supplemental FBS at 4 °C in the dark (data not shown).

In Figure 5, we present the absorption and fluorescence emission spectra of the OVG-10 constructs suspended in cell culture medium immediately postfabrication and after 79 days of storage in medium without and with 10% supplemental FBS. After 79 days of storage in the cell culture medium without supplemental FBS, there was up to a 25% reduction in absorbance over the 675−875 nm spectral band (Figure 5a), suggesting some ICG leakage over this time interval. In contrast to the reduction in absorbance, the peak fluorescence emission intensity of the resuspended OVG-10 constructs in response to 750 nm excitation was increased by ≈30% after 79 days of incubation in FBS -free culture medium (Figure 5b). Because the OVG-10 constructs were intentionally fabricated to have diminished fluorescence, the increased fluorescence intensity after 79 days of storage further suggests that some ICG leaked from within the constructs over this time interval to reduce the concentration of the entrapped ICG, restoring fluorescence

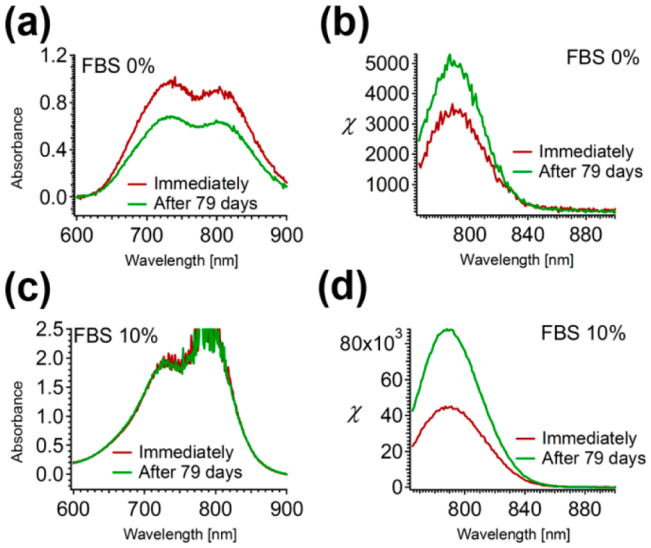

Figure 5. Absorption and fluorescence spectra of OVG-10 constructs in McCoy's 5A cell culture medium without and with 10% supplemental FBS taken immediately and at 79 days postfabrication. Panels a and b correspond to the absorbance and fluorescence spectra, respectively, of the OVGs in the medium without FBS. Panels c and d correspond to the absorbance and fluorescence spectra, respectively, of the OVGs in the medium supplemented with 10% FBS. The fluorescence spectra were obtained in response to excitation at λ = 750 nm.

emission. The fluorescence emission intensity of ICG is enhanced when its concentration decreases below 0.6−4 μM.[54,55]

In comparison to the absorbance of the OVG-10 constructs incubated in the cell culture medium without supplemental FBS (Figure 5a), the absorbance of the constructs incubated in the cell culture medium with 10% FBS increased and reached saturation levels in the 770−810 nm range (Figure 5c). This absorbance enhancement is similar to the increased absorbance effect associated with the OVG-40 constructs in the suspension buffer containing FBS (Figure 2a). The enhanced absorbance of the OVG-10 constructs remained persistent after 79 days of incubation in the cell culture medium supplemented with 10% FBS. There was an increase in the fluorescence emission intensity of the OVG-10 constructs incubated in the cell culture medium with 10% FBS level after 79 days (Figure 5d), which again can be attributed to a partial ICG leakage from the constructs over this time interval. We offer an explanation for the enhanced and persistent NIR absorption over 79 days (despite some ICG leakage) on the basis of eq 4, where the effective molar extinction coefficient and hence absorbance is a function of the sum of the products of the molar extinction coefficients and the fractions of ICG in its various conformations (i.e., unbound or bound). Therefore, a reduction in the ICG concentration within the OVGs resulting from leakage can be compensated for by an increased molar extinction coefficient (resulting from a new conformational state) to give rise to the same absorbance value.

The optical stability of nonencapsulated ICG in serum protein has been previously studied. Although the spectral absorbance of ICG in water was reduced by 10% after 10 h, the spectral absorbance of ICG in whole blood or in water containing 0.25−4% HSA was reduced by less than 2% after 10

h.[56,88] This ICG optical stability is attributed to the high binding affinity of ICG to albumin.

Effects of Serum Proteins on the OVG Size Distribution. When incubated in McCoy's 5A cell culture medium (I = 0.130 mol/L) without supplemental FBS, the peak size associated with 25% of the OVG-5 constructs and the full-width-at-half-max (fwhm) size were ≈2 and 1.02 μm, respectively (Figure 6). Because the diameter of a single

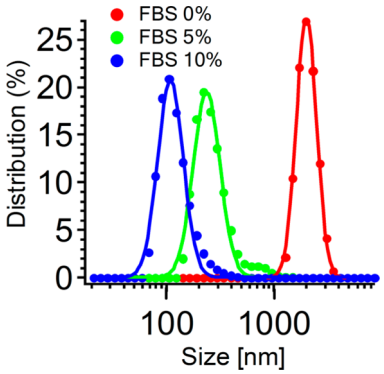

Figure 6. Hydrodynamic diameter distribution of the OVG-5 constructs in McCoy's 5A cell culture medium without and with supplemental FBS. Measurements (circles) were obtained by dynamic light scattering at room temperature in the dark. The curves are lognormal fits to the measured data.

OVG is about 25 nm,[23] this increase in size to levels that are on the order of micrometers is indicative of the aggregation of the constructs when incubated in cell culture medium without supplemental FBS. With increased levels of FBS to 5 and 10% in the cell culture medium, the fwhm sizes were substantially reduced to 134 and 67 nm, respectively. Nearly 21% of the OVGs in the cell culture medium supplemented with 10% FBS had an aggregation size of ≈100 nm (Figure 6).

We attribute the reduction in the aggregate size to the adsorption of serum proteins, mostly BSA in FBS, onto the surface of the OVGs by electrostatic interactions between the positively charged CP subunits and negatively charged BSA. Serum proteins surface adsorption leads to increased separation distances among OVGs by steric effects and electrostatic repulsions. These results also suggest that the serum proteins not only can interact with ICG within the constructs but also with the CP subunits on the surface of OVGs.

The progressive decrease in the aggregation of the OVGs with increased levels of FBS in cell culture medium is in good agreement with other studies. It has been recently reported that the Roswell Park Memorial Institute cell culture medium (I = 0.151 mol/L)[89] induced the aggregation of TiO2, silver, and gold NPs in a serum-protein-free environment. However, in cell culture medium containing serum, the protein-coated TiO2, silver, and gold NPs became dispersed.[42−44,90]

CONCLUSIONS

We have demonstrated that the absorption and fluorescence emission of OVGs are enhanced in biological media containing serum proteins. OVGs remain physically stable and maintain their NIR absorption and fluorescence properties in cell culture medium for at least 79 days (the time period investigated here). The presence of serum proteins reduces the aggregation of the OVGs. These findings are important in relation to the development of optical imaging and phototherapeutic methods on the basis of OVG as well as the expected optical and physical characteristics of these nanomaterials in vivo.

EXPERIMENTAL SECTION

Reagents. McCoy's 5A cell culture medium, which contains various inorganic salts (predominantly KCl, NaCl, and Na_2HPO_4), amino acids (predominantly L-glutamine), vitamins, and other macromolecules (predominantly D-glucose) was purchased from ATCC (30-2007, Manassa, VA). Fetal bovine serum (FBS) was purchased from Invitrogen (Grand Island, NY). Indocyanine green (ICG, powder, Sigma-Aldrich) was used as received. We initially prepared a stock solution of ICG (645 mM) in deionized water and subsequently used it for OVG fabrication. The OVG suspension buffer (50 mM NaAc, 8 mM MgAc, pH 4) was prepared and stored at 4 °C.

Fabrication of OVGs. We previously reported the detailed procedure for the fabrication of OVGs.[23] Briefly, BMV-infected barley leaves were collected and ground thoroughly in BMV extraction buffer (0.5 M NaAc and 0.08 M MgAc, pH 4). The extract was centrifuged in chloroform at ≈11 000g (type 45 Ti rotor, Optima XPN-90, Beckman Coulter, Brea, CA) for 15 min at room temperature. The supernatant was centrifuged at ≈70 000g (type 45 Ti rotor, Optima XPN-90) for 3 h. The pellet was subject to 5−25% sucrose density gradient centrifugation. The purified virus solution was dialyzed against 1 L of disassembly buffer (0.5 M $CaCl_2$, 50 mM Tris-HCl, 1 mM EDTA, 1 mM dithiothreitol (DTT), and 0.5 mM phenylmethylsulfonyl fluoride (PMSF), pH 7.5) for 24 h at 4 °C. The solution from the dialysis bag was centrifuged at ≈21 000g (Eppendorf centrifuge 5424R, Hauppauge, NY) for 30 min to pellet the viral RNA and nondissociated BMV. The supernatant was then centrifuged at ≈261 000g (type 90 Ti rotor, Optima XPN-90) for 1 h at 4 °C to pellet any undissociated virus particles. The supernatant, which contains the CP subunits of BMV, was dialyzed against the RNA assembly buffer (50 mM NaCl, 50 mM Tris-HCl, 10 mM KCl, 5 mM MgCl2, and 1 mM DTT, pH 7.2) for 24 h at 4 °C. This step ensures the complete removal of the RNA during the synthesis of OVGs because RNA-containing virions will only form at neutral pH. The solution was then collected and centrifuged at ≈261 000g (type 90 Ti rotor, Optima XPN-90) for 1 h to pellet RNA-containing virions. The supernatant contained the purified CPs, which can be used immediately or stored at 4 °C for 1 to 2 weeks. The concentration of the CP subunits was determined from the absorbance value at 280 nm. ICG was added to the purified suspension of the CP subunits, and the mixture was dialyzed against the reassembly buffer (1 M NaCl, 50 mM NaAc, 1 mM EDTA, and 1 mM DTT, pH 4.8) at 4 °C for 24 h. All aqueous buffer solutions were made from deionized and distilled water.

We define ϕ as the ratio of BMV CPs concentration to that of ICG used during the OVG assembly process. We fabricated various sets of OVGs: OVG-120 (ϕ = 120, ICG concentration = 13 μM), OVG-40 (ϕ = 40, ICG concentration = 13 μM), OVG-10 (ϕ = 10, ICG concentration = 74 μM), OVG-5 (ϕ = 5, ICG concentration = 184.5 μM), and OVG-4 (ϕ = 4, ICG concentration = 31 μM). The dialyzed solution was centrifuged at 261 000g for 1 h to pellet the OVGs. We discarded the supernatant, which may contain excess unbound ICG. OVG suspension buffer was added into the pellet to allow immediate resuspension by vortexing or overnight storage at 4 °C.

OVG Suspension Buffer and Its Supplemental Ingredients. The OVG-40 and OVG-120 constructs in OVG suspension buffer (pH 4.3) were supplemented with different levels of FBS (5 or 10% v/v). Because bovine serum albumin (BSA) has the highest relative concentration among the proteins in FBS,[91−93] we also prepared OVG suspension buffers supplemented with BSA at different concentration levels (0.06−0.60 mM).

We obtained the absorption and fluorescence spectra of the constructs immediately after exposure to each of the FBS and BSA conditions (further details will follow). As control experiments, we obtained the absorption and fluorescence spectra of ICG in the OVG suspension buffer without and with FBS or BSA at the same levels as above.

Optical Absorption and Fluorescence Spectroscopy. The optical absorption spectra of OVGs and nonencapsulated ICG were obtained in the 230−900 nm spectral range using a UV−vis−Near-IR (UV−vis−NIR) spectrometer (Cary 50, Varian Inc.). NIR fluorescence emission spectra of the OVGs and nonencapsulated ICG (control) in the range of 765−900 nm were obtained in response to a 750 nm excitation light (from a monochromator and a Xenon arc lamp) and were recorded by a fluorescence spectrophotometer (Fluorolog 3, Horiba Jobin Yvon, Edison, NJ). The 750 nm excitation wavelength was chosen to elicit fluorescence from the monomer form of ICG.

The fluorescence emission spectra were normalized to absorption at the excited wavelength as

$$\zeta(\lambda) = \frac{F(\lambda)}{1 - 10^{-A}} \quad (5)$$

where $F(\lambda)$ is the wavelength (λ)-dependent fluorescence emission intensity and A is the absorbance value at the excitation wavelength (750 nm).

Ionic Strength (*I*) of the Solutions. We calculated the ionic strength for the OVG suspension buffer and cell culture medium using the following equation[94]

$$I = \frac{1}{2}\sum_{i=1}^{n} C_i \times Z_i^2 \quad (6)$$

where C_i is the molar concentration (mol/L) of each ion in the solution and Z_i is the respective charge. Using this equation, the respective I values for the OVG buffer solution and McCoy's 5A culture medium were 0.074 and 0.130 mol/L.

Transmission Electron Microscopy (TEM). OVGs were placed onto 400 mesh carbon-Formvar grids (01814-F, Ted Pella Inc., Redding, CA) for 7 min. The grids were rinsed with water, wicked dry, and stained with a 2% uranyl acetate for 7 min. The samples were viewed at 300 kV using a Philips CM300 TEM system at 19 500−51 000× magnification. The images were collected as 1024 × 1024 pixel 14-bit gray-scale Gatan Digital Micrograph 3 (DM3) files using a Gatan 794 CCD multiscan camera, and they were converted into 8-bit gray-scale TIF files.

Stability Assessment of the OVGs. To assess the physical and optical stability of OVGs, we intentionally fabricated OVG constructs (OVG-10) in which the fluorescence was diminished by encapsulating a large amount of ICG. The constructs were incubated at 4 °C in cell culture medium containing 5% supplemental FBS for 24 h in the dark. After 24 h of incubation, we obtained images of the OVG-10 constructs in response to white-light (broadband) illumination and NIR excitation (740 ± 10 nm, Prophotonix, Salem, NH). The images in response to while-light illumination were captured by an Olympus digital camera. A filter was used to pass the emitted NIR light at wavelengths >810 nm, which was then detected by a CCD camera (Pixis 1024B, Roper Scientific GmbH Germany) with an exposure time of 0.5 s.

To assess the optical stability of OVGs over a longer time, we incubated the OVG-10 constructs in cell culture medium without and with 10% supplemental FBS for 79 days in the dark at 4 °C. The absorption and fluorescence spectra of the constructs were then obtained after 79 days of incubation.

Measurements of the Aggregate Size. We assessed the aggregation of OVG-5 constructs in McCoy's 5A cell culture medium supplemented with 0, 5, and 10% FBS by dynamic light scattering (DLS) (Malvern Zetasizer Nano, Worcestershire, UK). We fitted the measured size distributions with lognormal functions. DLS was performed in room temperature in the dark.

AUTHOR INFORMATION

Corresponding Author

*E-mail: anvarib@ucr.edu.

Notes

The authors declare no competing financial interest.

ACKNOWLEDGMENTS

This work was supported by the National Science Foundation (CBET-1144237) and the Bioengineering Center at the University of California, Riverside (UCR). The electron microscopy images were obtained at the Central Facility for Advanced Microscopy and Microanalysis (CFAMM) at UCR. We used the public protein data bank (http://www.rcsb.org) to obtain the albumin structure to generate the figure for the Table of Contents.

REFERENCES

(1) Altinoglu, E. I.; Adair, J. H. *Wiley Interdiscip. Rev.: Nanomed. Nanobiotechnol.* **2010**, *2*, 461−477.

(2) Melancon, M. P.; Zhou, M.; Li, C. *Acc. Chem. Res.* **2011**, *44*, 947−956.

(3) Pansare, V. J.; Hejazi, S.; Faenza, W. J.; Prud'homme, R. K. *Chem. Mater.* **2012**, *24*, 812−827.

(4) Aswathy, R. G.; Yoshida, Y.; Maekawa, T.; Kumar, D. S. *Anal. Bioanal. Chem.* **2010**, *397*, 1417−1435.

(5) Weissleder, R. *Nat. Biotechnol.* **2001**, *19*, 316−317.

(6) Wang, Y. Q.; Chen, L. X. *Nanomedicine* **2011**, *7*, 385−402.

(7) Gao, X. H.; Cui, Y. Y.; Levenson, R. M.; Chung, L. W. K.; Nie, S. M. *Nat. Biotechnol.* **2004**, *22*, 969−976.

(8) Kim, S.; Lim, Y. T.; Soltesz, E. G.; De Grand, A. M.; Lee, J.; Nakayama, A.; Parker, J. A.; Mihaljevic, T.; Laurence, R. G.; Dor, D. M.; Cohn, L. H.; Bawendi, M. G.; Frangioni, J. V. *Nat. Biotechnol.* **2004**, *22*, 93−97.

(9) Cai, W. B.; Hsu, A. R.; Li, Z. B.; Chen, X. Y. *Nanoscale Res. Lett.* **2007**, *2*, 265−281.

(10) Resch-Genger, U.; Grabolle, M.; Cavaliere-Jaricot, S.; Nitschke, R.; Nann, T. *Nat. Methods* **2008**, *5*, 763−775.

(11) Derfus, A. M.; Chan, W. C. W.; Bhatia, S. N. *Nano Lett.* **2004**, *4*, 11−18.

(12) Ryman-Rasmussen, J. P.; Riviere, J. E.; Monteiro-Riviere, N. A. *J. Invest. Dermatol.* **2007**, *127*, 143−153.

(13) Derycke, A. S. L.; Kamuhabwa, A.; Gijsens, A.; Roskams, T.; De Vos, D.; Kasran, A.; Huwyler, J.; Missiaen, L.; de Witte, P. A. M. *J. Natl. Cancer Inst.* **2004**, *96*, 1620−1630.

(14) Song, L. P.; Li, H.; Sunar, U.; Chen, J.; Corbin, I.; Yodh, A. G.; Zheng, G. *Int. J. Nanomed.* **2007**, *2*, 767−774.

(15) Cho, H.; Indig, G. L.; Weichert, J.; Shin, H. C.; Kwon, G. S. *Nanomedicine* **2012**, *8*, 228−236.

(16) Kirchherr, A. K.; Briel, A.; Mader, K. *Mol. Pharmaceutics* **2009**, *6*, 480−491.

(17) Rodriguez, V. B.; Henry, S. M.; Hoffman, A. S.; Stayton, P. S.; Li, X. D.; Pun, S. H. *J. Biomed. Opt.* **2008**, *13*, 014025.

(18) Saxena, V.; Sadoqi, M.; Shao, J. *J. Photochem. Photobiol., B* **2004**, *74*, 29−38.

(19) Ghoroghchian, P. P.; Frail, P. R.; Susumu, K.; Blessington, D.; Brannan, A. K.; Bates, F. S.; Chance, B.; Hammer, D. A.; Therien, M. J. *Proc. Natl. Acad. Sci. U.S.A.* **2005**, *102*, 2922−2927.

(20) Saxena, V.; Sadoqi, M.; Shao, J. *Int. J. Pharm. (Amsterdam, Neth.)* **2006**, *308*, 200−204.

(21) Yu, J.; Javier, D.; Yaseen, M. A.; Nitin, N.; Richards-Kortum, R.; Anvari, B.; Wong, M. S. *J. Am. Chem. Soc.* **2010**, *132*, 1929−1938.

(22) Yu, J.; Yaseen, M. A.; Anvari, B.; Wong, M. S. *Chem. Mater.* **2007**, *19*, 1277−1284.

(23) Jung, B. S.; Rao, A. L. N.; Anvari, B. *ACS Nano* **2011**, *5*, 1243−1252.

(24) Aniagyei, S. E.; DuFort, C.; Kao, C. C.; Dragnea, B. *J. Mater. Chem.* **2008**, *18*, 3763−3774.

(25) Sikkema, F. D.; Comellas-Aragones, M.; Fokkink, R. G.; Verduin, B. J. M.; Cornelissen, J.; Nolte, R. J. M. *Org. Biomol. Chem.* **2007**, *5*, 54−57.

(26) Kaiser, C. R.; Flenniken, M. L.; Gillitzer, E.; Harmsen, A. L.; Harmsen, A. G.; Jutila, M. A.; Douglas, T.; Young, M. J. *Int. J. Nanomed.* **2007**, *2*, 715−733.

(27) Singh, P.; Prasuhn, D.; Yeh, R. M.; Destito, G.; Rae, C. S.; Osborn, K.; Finn, M. G.; Manchester, M. *J. Controlled Release* **2007**, *120*, 41−50.
(28) Pokorski, J. K.; Steinmetz, N. F. *Mol. Pharmaceutics* **2010**, *8*, 29−43.
(29) Destito, G.; Schneemann, A.; Manchester, M. In *Viruses and Nanotechnology*; Manchester, M., Steinmetz, N. F., Eds.; Springer-Verlag: Berlin, Germany, 2009; Vol. *327*, pp 95−122.
(30) Steinmetz, N. F. *Nanomedicine* **2010**, *6*, 634−641.
(31) Yildiz, I.; Shukla, S.; Steinmetz, N. F. *Curr. Opin. Biotechnol.* **2011**, *22*, 901−908.
(32) Young, M.; Willits, D.; Uchida, M.; Douglas, T. *Annu. Rev. Phytopathol.* **2008**, *46*, 361−384.
(33) Dixit, S. K.; Goicochea, N. L.; Daniel, M. C.; Murali, A.; Bronstein, L.; De, M.; Stein, B.; Rotello, V. M.; Kao, C. C.; Dragnea, B. *Nano Lett.* **2006**, *6*, 1993−1999.
(34) Goicochea, N. L.; De, M.; Rotello, V. M.; Mukhopadhyay, S.; Dragnea, B. *Nano Lett.* **2007**, *7*, 2281−2290.
(35) Chen, C.; Daniel, M. C.; Quinkert, Z. T.; De, M.; Stein, B.; Bowman, V. D.; Chipman, P. R.; Rotello, V. M.; Kao, C. C.; Dragnea, B. *Nano Lett.* **2006**, *6*, 611−615.
(36) Huang, X. L.; Bronstein, L. M.; Retrum, J.; Dufort, C.; Tsvetkova, I.; Aniagyei, S.; Stein, B.; Stucky, G.; McKenna, B.; Remmes, N.; Baxter, D.; Kao, C. C.; Dragnea, B. *Nano Lett.* **2007**, *7*, 2407−2416.
(37) Lewis, J. D.; Destito, G.; Zijlstra, A.; Gonzalez, M. J.; Quigley, J. P.; Manchester, M.; Stuhlmann, H. *Nat. Med.* **2006**, *12*, 354−360.
(38) Steinmetz, N. F.; Mertens, M. E.; Taurog, R. E.; Johnson, J. E.; Commandeur, U.; Fischer, R.; Manchester, M. *Nano Lett.* **2010**, *10*, 305−312.
(39) Loo, L.; Guenther, R. H.; Lommel, S. A.; Franzen, S. *Chem. Commun.* **2008**, 88−90.
(40) Basu, S.; Ghosh, S. K.; Kundu, S.; Panigrahi, S.; Praharaj, S.; Pande, S.; Jana, S.; Pal, T. *J. Colloid Interface Sci.* **2007**, *313*, 724−734.
(41) Cedervall, T.; Lynch, I.; Foy, M.; Berggad, T.; Donnelly, S. C.; Cagney, G.; Linse, S.; Dawson, K. A. *Angew. Chem., Int. Ed.* **2007**, *46*, 5754−5756.
(42) Mahl, D.; Greulich, C.; Meyer-Zaika, W.; Koller, M.; Epple, M. *J. Mater. Chem.* **2010**, *20*, 6176−6181.
(43) Kittler, S.; Greulich, C.; Gebauer, J. S.; Diendorf, J.; Treuel, L.; Ruiz, L.; Gonzalez-Calbet, J. M.; Vallet-Regi, M.; Zellner, R.; Koller, M.; Epple, M. *J. Mater. Chem.* **2010**, *20*, 512−518.
(44) Dobrovolskaia, M. A.; Patri, A. K.; Zheng, J. W.; Clogston, J. D.; Ayub, N.; Aggarwal, P.; Neun, B. W.; Hall, J. B.; McNeil, S. E. *Nanomedicine* **2009**, *5*, 106−117.
(45) Monopoli, M. P.; Walczyk, D.; Campbell, A.; Elia, G.; Lynch, I.; Bombelli, F. B.; Dawson, K. A. *J. Am. Chem. Soc.* **2011**, *133*, 2525−2534.
(46) Cedervall, T.; Lynch, I.; Lindman, S.; Berggard, T.; Thulin, E.; Nilsson, H.; Dawson, K. A.; Linse, S. *Proc. Natl. Acad. Sci. U.S.A.* **2007**, *104*, 2050−2055.
(47) Kim, J. S.; Lee, C.; Foxworth, A.; Waldman, T. *Cancer Res.* **2004**, *64*, 1932−1937.
(48) Philip, R.; Penzkofer, A.; Baumler, W.; Szeimies, R. M.; Abels, C. *J. Photochem. Photobiol., A* **1996**, *96*, 137−148.
(49) Mauerer, M.; Penzkofer, A.; Zweck, J. *J. Photochem. Photobiol., B* **1998**, *47*, 68−73.
(50) Gelamo, E. L.; Tabak, M. *Spectrochim. Acta, Part A* **2000**, *56*, 2255−2271.
(51) Steinhardt., J.; Krijn, J.; Leidy, J. G. *Biochemistry* **1971**, *10*, 4005−4015.
(52) Zhou, J. F.; Chin, M. P.; Schafer, S. A. In *Proc. SPIE*; The Society: Bellingham, WA, 1994; Vol. *2128*, pp 495−505.
(53) Mordon, S.; Devoisselle, J. M.; Soulie-Begu, S.; Desmettre, T. *Microvasc. Res.* **1998**, *55*, 146−152.
(54) Benson, R. C.; Kues, H. A. *Phys. Med. Biol.* **1978**, *23*, 159−163.
(55) Desmettre, T.; Devoisselle, J. M.; Mordon, S. *Surv. Ophthalmol.* **2000**, *45*, 15−27.
(56) Landsman, M. L. J.; Kwant, G.; Mook, G. A.; Zijlstra, W. G. *J. Appl. Physiol.* **1976**, *40*, 575−583.
(57) Cherrick, G. R.; Stein, S. W.; Leevy, C. M.; Davidson, C. S. *J. Clin. Invest.* **1960**, *39*, 592−600.
(58) Herz, A. H. *Adv. Colloid Interface Sci.* **1977**, *8*, 237−298.
(59) Kasha, M.; Rawls, H. R.; Ashraf El-bayoumi, M. *Pure Appl. Chem.* **1965**, *11*, 371−392.
(60) Berezin, M. Y.; Lee, H.; Akers, W.; Nikiforovich, G.; Achilefu, S. *Photochem. Photobiol.* **2007**, *83*, 1371−1378.
(61) Ogawa, M.; Kosaka, N.; Choyke, P. L.; Kobayashi, H. *ACS Chem. Biol.* **2009**, *4*, 535−546.
(62) Vandergraaf, M.; Vanmierlo, C. P. M.; Hemminga, M. A. *Biochemistry* **1991**, *30*, 5722−5727.
(63) Cuillel, M.; Berthetcolominas, C.; Timmins, P. A.; Zulauf, M. *Eur. Biophys. J.* **1987**, *15*, 169−176.
(64) Pfeiffer, P.; Herzog, M.; Hirth, L. *Philos. Trans. R. Soc., B* **1976**, *276*, 99−107.
(65) Incardon., N. L.; McKee, S.; Flanegan, J. B. *Virology* **1973**, *53*, 204−214.
(66) Pfeiffer, P.; Durham, A. C. H. *Virology* **1977**, *81*, 419−432.
(67) Zulauf, M. *J. Mol. Biol.* **1977**, *114*, 259−266.
(68) Kratz, F. *J. Controlled Release* **2008**, *132*, 171−183.
(69) Wiogo, H. T. R.; Lim, M.; Bulmus, V.; Yun, J.; Amal, R. *Langmuir* **2011**, *27*, 843−850.
(70) Erickson, H. P. *Biol. Proced. Online* **2009**, *11*, 32−51.
(71) Jacrot, B.; Chauvin, C.; Witz, J. *Nature* **1977**, *266*, 417−421.
(72) Chauvin, C.; Pfeiffer, P.; Witz, J.; Jacrot, B. *Virology* **1978**, *88*, 138−148.
(73) Anderegg, J. W.; Wright, M.; Kaesberg, P. *Biophys. J.* **1963**, *3*, 175−182.
(74) Casselyn, M.; Perez, J.; Tardieu, A.; Vachette, P.; Witz, J.; Delacroix, H. *Acta Crystallogr., Sect. D* **2001**, *57*, 1799−1812.
(75) Baker, T. S.; Olson, N. H.; Fuller, S. D. *Microbiol. Mol. Biol. Rev.* **1999**, *63*, 862−922.
(76) Lucas, R. W.; Larson, S. B.; McPherson, A. *J. Mol. Biol.* **2002**, *317*, 95−108.
(77) Larson, S. B.; Lucas, R. W.; McPherson, A. *J. Mol. Biol.* **2005**, *346*, 815−831.
(78) Lucas, R. W.; Kuznetsov, Y. G.; Larson, S. B.; McPherson, A. *Virology* **2001**, *286*, 290−303.
(79) Lavelle, L.; Michel, J. P.; Gingery, M. *J. Virol. Methods* **2007**, *146*, 311−316.
(80) Soto, C. M.; Ratna, B. R. *Curr. Opin. Biotechnol.* **2010**, *21*, 426−438.
(81) Speir, J. A.; Munshi, S.; Wang, G. J.; Baker, T. S.; Johnson, J. E. *Structure* **1995**, *3*, 63−78.
(82) Singh, P.; Gonzalez, M. J.; Manchester, M. *Drug Dev. Res.* **2006**, *67*, 23−41.
(83) Douglas, T.; Young, M. *Nature* **1998**, *393*, 152−155.
(84) Hooker, J. M.; Kovacs, E. W.; Francis, M. B. *J. Am. Chem. Soc.* **2004**, *126*, 3718−3719.
(85) Valegard, K.; Liljas, L.; Fridborg, K.; Unge, T. *Nature* **1990**, *345*, 36−41.
(86) Sherman, M. B.; Guenther, R. H.; Tama, F.; Sit, T. L.; Brooks, C. L.; Mikhailov, A. M.; Orlova, E. V.; Baker, T. S.; Lommel, S. A. *J. Virol.* **2006**, *80*, 10395−10406.
(87) Cuillel, M.; Jacrot, B.; Zulauf, M. *Virology* **1981**, *110*, 63−72.
(88) Gathje, J.; Steuer, R. R.; Nicholes, K. R. *J. Appl. Physiol.* **1970**, *29*, 181−185.
(89) Phenrat, T.; Long, T. C.; Lowry, G. V.; Veronesi, B. *Environ. Sci. Technol.* **2009**, *43*, 195−200.
(90) Allouni, Z. E.; Cimpan, M. R.; Hol, P. J.; Skodvin, T.; Gjerdet, N. R. *Colloids Surf., B* **2009**, *68*, 83−87.
(91) Testerman, T. L.; McGee, D. J.; Mobley, H. L. T. *J. Clin. Microbiol.* **2001**, *39*, 3842−3850.
(92) Bertolero, F.; Kaighn, M. E.; Camalier, R. F.; Saffiotti, U. *In Vitro Cell. Dev. Biol.* **1986**, *22*, 423−428.
(93) Zheng, X. Y.; Baker, H.; Hancock, W. S.; Fawaz, F.; McCaman, M.; Pungor, E. *Biotechnol. Prog.* **2006**, *22*, 1294−1300.

(94) Morais, S.; Carvalho, G. S.; Sousa, J. P. *Electroanalysis* **1996**, *8*, 1174−1178.